Rate-equation approach to island size distributions and capture numbers in submonolayer irreversible growth

Mihail N. Popescu,[1] Jacques G. Amar,[2] and Fereydoon Family[1]
[1]*Department of Physics, Emory University, Atlanta, Georgia 30322*
[2]*Department of Physics & Astronomy, University of Toledo, Toledo, Ohio 43606*
(Received 14 December 2000; revised manuscript received 25 April 2001; published 19 October 2001)

We present a quantitative rate-equation approach to irreversible submonolayer growth on a two-dimensional substrate. Our method explicitly takes into account the existence of a denuded (''capture'') zone around every island and the correlations between the size of an island and the corresponding average capture zone. The evolution of the capture-zone distributions is described by a set of Voronoi-area evolution equations, which are coupled to the usual rate equations for the island densities through local rates of monomer capture. The combined set of equations leads to a fully self-consistent calculation of the size- and coverage-dependent capture numbers. The resulting predictions for the average capture-zone and capture-number distributions are in excellent agreement with experimental results and Monte Carlo simulations. As a result, the corresponding scaled island size distributions and their dependence on coverage and deposition rate are also accurately predicted in the precoalescence regime.

DOI: 10.1103/PhysRevB.64.205404 PACS number(s): 81.15.Aa, 68.55.−a, 68.35.Bs, 82.40.Bj

I. INTRODUCTION

Molecular-beam epitaxy (MBE) offers the possibility of atomic-scale controlled production of thin films, high-quality crystals, and nanostructures.[1] The submonolayer growth in MBE involves nucleation, aggregation, and coalescence of islands leading to a distribution of islands of various sizes and morphologies. The morphology and the spatial distribution of the islands determines the quality of the desired nanostructure (quantum dots/wires) or of the multilayer growth (thin films). These nanoscale features of the surface in the early stages of MBE growth can now be measured in real-time with atomic-scale resolution experimental methods, such as scanning tunneling microscopy (STM) and reflection high-energy electron diffraction (RHEED).[1] This has led to a renewed experimental interest in submonolayer nucleation and growth,[2–13] and has also stimulated considerable theoretical work toward a better understanding of the mechanisms determining the scaling properties of the island density and island-size distribution in epitaxial growth.[14–34]

One of the standard tools used in theoretical studies of submonolayer growth is the rate-equation (RE) approach.[14,35,36] It involves a set of deterministic, coupled reaction-diffusion equations describing the time (coverage) dependence of average quantities through a set of rate coefficients usually called capture numbers.[14,35] While simple mean-field choices for the capture numbers lead to correct predictions for the scaling behavior of the island and monomer densities as a function of deposition flux and temperature, in order to make quantitative predictions accurate expressions for the rate coefficients should be used.

Recently, Bales and Chrzan[20] have developed a self-consistent RE approach that leads to quantitative predictions for the average monomer and island capture numbers, as well as for the average island and monomer densities in two-dimensional irreversible growth. This approach has also recently been extended to the case of reversible growth,[21,33] but neither for reversible nor for irreversible growth does it lead to correct predictions for the island-size distributions.[20,21,24,33] The reason is that it is based on a mean-field approximation, which ignores spatial and temporal correlations in the growth of islands.[23,30,31]

In this paper we present a rate-equation approach to two-dimensional irreversible submonolayer growth in which the existence of a denuded (''capture'') zone and the correlations between the size of the island and the corresponding average capture zone are explicitly taken into account. A second set of equations is used to describe the evolution of the island-size-dependent capture zones, leading to explicit size- and coverage-dependent capture numbers $\sigma_s(\theta)$ in good agreement with experimental[31] and simulation results.[27] A numerical solution of the resulting island-density rate equations leads to island-size distributions in good agreement with simulations, in contrast to the standard rate-equation approach.

We note that a general outline of our method and results has already been presented in Ref. 34. Here we present a detailed derivation of the relevant equations along with explicit analytical expressions for the local capture number, monomer density distribution, and self-consistency conditions. In addition, a detailed study of the dependence of the island-size distribution, capture-number distribution, and average capture zone ''distribution'' on the island morphology is presented along with a study of the evolution of the island-size distribution as a function of coverage and deposition rate. A possible generalization of our method for the case of reversible growth is also discussed.

The organization of this paper is as follows. Section II presents the details of the self-consistent calculation of the capture numbers. After a brief introduction to the rate-equation formalism, the geometry of the exclusion zones is defined and the local capture number is calculated as a function of the corresponding Voronoi area. It is then shown that both the coverage dependence of the capture number and island-size correlations are naturally included through the av-

eraging over the distribution of Voronoi areas. This part concludes with a discussion of self-consistency conditions and of their connection with the geometry of the system. In Sec. III, evolution equations for the Voronoi areas are developed and solved in closed form. We then discuss, in Sec. IV, our rate-equation results and present comparisons with experimental as well as kinetic Monte Carlo (KMC) results. A summary of our results and conclusions is presented in Sec. V.

II. SELF-CONSISTENT THEORY OF SIZE-DEPENDENT CAPTURE NUMBERS

A. Rate equations

A rate-equation approach to submonolayer nucleation and growth involves a set of deterministic, coupled, diffusion-aggregation equations describing the time (coverage) dependence of average quantities.[14,35,36] The RE variables are the average densities of monomers, N_1, and of islands of size $s \geqslant 2$, N_s, where s is the number of atoms in the island. A general form of these equations for irreversible growth may be written as

$$\frac{dN_1}{d\theta} = \gamma - 2N_1 - 2R\sigma_1 N_1^2 - RN_1 \sum_{s\geqslant 2} \sigma_s N_s, \qquad (1)$$

$$\frac{dN_s}{d\theta} = RN_1(\sigma_{s-1}N_{s-1} - \sigma_s N_s) + k_{s-1}N_{s-1} - k_s N_s \quad \text{for } s \geqslant 2, \qquad (2)$$

where θ is the coverage, γ is the fraction of the substrate not covered by islands, σ_s are the capture numbers, and k_s are the rates of deposition on top of existing islands. Here, the kinetic constant $R = D/F$ is the ratio of the diffusion constant D (where $D = D_h/4$ for the case of nearest-neighbor hopping with isotropic hopping rate D_h on a two-dimensional lattice) to the deposition flux F. The terms with σ_s describe the rate of monomer capture by other monomers or by existing islands. The terms with k_s, where $k_s = s^{2/d_f}$ and d_f is the fractal dimension of the islands,[20] correspond to the deposition of adatoms directly on islands of size s. Finally, the quantity $\gamma - 2N_1$ corresponds to the deposition flux minus the direct impingement.

In order to study the effects of island morphology on the capture-number and island-size distributions, we consider two different models: a *point-island* model and an *extended-island* model. In the *point-island* model, each island occupies just one lattice site. Dimer nucleation occurs when two monomers land on the same site, while any monomer that lands on the site occupied by an island becomes part of the island. Physically, this corresponds to islands that grow only in a direction perpendicular to the substrate, or, alternatively, to islands with a very large fractal dimension ($d_f = \infty$). For point islands the fraction of the substrate not covered by islands is then given by $\gamma = 1 - N$, where $N = \Sigma_{s\geqslant 2} N_s$ is the total island density.

In the *extended-island* model, an island occupies a number of lattice sites equal to its size s, and monomers attach to a growing island or to another monomer at the nearest-neighbor perimeter sites. Depending on the details of the growth, the resulting islands can have a compact shape ($d_f = 2$) or a fractal morphology ($d_f < 2$). For extended islands the factor γ is given by $\gamma = 1 - \theta + N_1$.

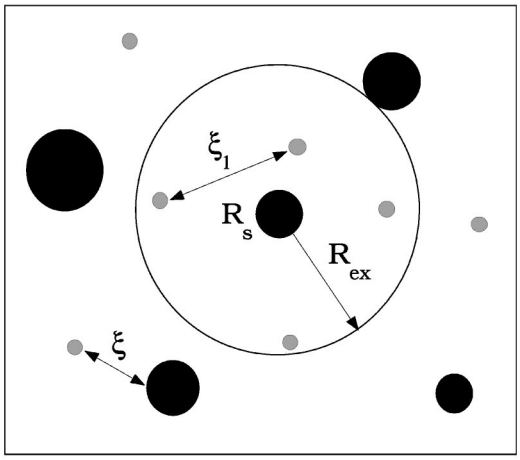

FIG. 1. Schematic representation of the capture-zone geometry for an island of size s (radius R_s). Shown are islands of different sizes (big dark circles), monomers (gray circles), the boundary of the exclusion zone (the circle of radius R_{ex}), and the nucleation and mean-field decay lengths ξ_1, respectively ξ.

Once the capture numbers $\sigma_s(\theta)$ are known, Eqs. (1) and (2) can be numerically solved to find the island-size distribution $N_s(\theta)$. However, understanding and predicting the size and coverage dependence of the capture numbers has been the central problem of the rate-equation theory of MBE growth[14,22,36–39] for more than three decades. In the next section we present a theoretical approach that allows an explicit calculation of the correct size- and coverage-dependent capture numbers.

B. Monomer-diffusion equation and local capture numbers

It has been argued that an island grows by collecting monomers mainly from a ''capture'' zone around the island,[25,27,31] and that these capture zones are related to the physically and geometrically well-defined Voronoi cells[23,27] corresponding to the set of points around an island closer to it than to its neighbors. As has already been noted, in order to quantitatively predict the coverage- and island-size dependence of the capture numbers σ_s, one needs to take into account these correlations between the size of the island and its local environment.

As shown in Fig. 1, these observations lead to the following model for the environment of an island. An island of size s is approximated by a circular region of radius $R_s = \rho s^{1/d_f}$, where ρ is a ''geometrical'' prefactor that accounts for the circular approximation of the island area and the fractal dimension d_f depends on the morphology of the island. The area surrounding the island is divided into an inner ($R_s < r < R_{ex}$) and an outer region ($R_{ex} < r < \infty$). The inner region corresponds to an exclusion zone in which only monomers can be found. The area of the exclusion zone A_{ex} is assumed to be proportional to the Voronoi area A_V of the Voronoi polygon surrounding the island, i.e., $A_{ex} = \eta A_V$, where the

factor η (typically larger than 1) is assumed to be the same for all islands. Accordingly, the radius of this zone is $R_{ex} = \sqrt{\eta} R_V$, where $R_V = \sqrt{A_V/\pi}$ is the ''radius'' of the Voronoi polygon. In the outer region, corresponding to $r > R_{ex}$, we assume a ''smeared'' uniform distribution of monomers and islands, which is independent of the size of the central island, as in Ref. 20.

This geometry naturally leads to the definition of a ''nucleation'' length ξ_1 and of a mean-field ''screening'' or monomer ''capture,'' length ξ. The nucleation length ξ_1 characterizes the monomer decay in the exclusion zone and is defined by

$$1/\xi_1^2 = 2\sigma_1 N_1. \tag{3}$$

Similarly, the mean-field screening length ξ, where

$$1/\xi^2 = 2\sigma_1 N_1 + \sum_{s \geqslant 2} \sigma_s N_s, \tag{4}$$

characterizes the monomer decay in the region *surrounding* the exclusion zone. Using these definitions, the monomer density rate equation (1) may be rewritten in the form

$$\frac{dN_1}{d\theta} = \gamma - 2N_1 - RN_1/\xi^2. \tag{5}$$

A self-consistent calculation of the capture numbers σ_s entering into the rate equations (1) and (2) is then based on comparing the microscopic capture rate of monomers near an island with the corresponding capture terms in the rate equations.[20,21] To determine the microscopic capture rate, we consider the following diffusion equation describing the *local* monomer density $n_1(\vec{r}, \theta)$:

$$\frac{\partial n_1}{\partial \theta} = \begin{cases} 1 - 2n_1 + R\nabla^2 n_1 - Rn_1/\xi_1^2, & R_s < r \leqslant R_{ex} \\ 1 - 2n_1 + R\nabla^2 n_1 - Rn_1/\xi^2, & r > R_{ex}. \end{cases} \tag{6}$$

The first two terms on the right side of Eq. (6) correspond to deposition minus direct impingement of monomers on monomers, while the last two terms correspond to monomer diffusion and, respectively, loss of monomers by nucleation[40,41] ($R_s < r \leqslant R_{ex}$) or by nucleation and aggregation ($r > R_{ex}$).

Multiplying Eq. (6) by γ and subtracting the monomer rate equation (5), one obtains

$$\nabla^2 n_1 - \frac{1}{\gamma R}\left(\gamma \frac{\partial n_1}{\partial \theta} - \frac{\partial N_1}{\partial \theta}\right) + \frac{2}{\gamma R}(\gamma n_1 - N_1) = \begin{cases} \xi_1^{-2}[n_1 - \alpha^2(N_1/\gamma)], & R_s < r \leqslant R_{ex} \\ \xi^{-2}(n_1 - N_1/\gamma), & r > R_{ex}, \end{cases} \tag{7}$$

where $\alpha^2 = (\xi_1/\xi)^2$. Since by definition γ represents the fraction of sites that are not occupied by islands, the proper normalization of the local monomer density is $\overline{n_1} = N_1/\gamma$, where $\overline{n_1}$ denotes the average local monomer density in the region between islands. This implies that the last term on the left-hand side of Eq. (7) may be neglected. Similarly, the quantity in the parentheses in the second term is also small and therefore in the limit of large R the second term may be neglected as well. This leads to the quasistatic monomer diffusion equation

$$\nabla^2 n_1 \simeq \begin{cases} \xi_1^{-2}[n_1 - \alpha^2(N_1/\gamma)] & \text{for } R_s < r \leqslant R_{ex} \\ \xi^{-2}(n_1 - N_1/\gamma) & \text{for } r > R_{ex}. \end{cases} \tag{8}$$

For the case of irreversible growth, the local monomer density $n_1(r)$ must vanish at the island edge and must also match the average local density (N_1/γ) far away from the island. In addition, the interior and exterior solutions must match at the exclusion-zone boundary. This leads to the following boundary conditions:

$$n_1(R_s) = 0, \tag{9a}$$

$$n_1(R_{ex}^-) = n_1(R_{ex}^+), \quad \nabla n_1(R_{ex}^-) = \nabla n_1(R_{ex}^+), \tag{9b}$$

$$\lim_{r \to \infty} n_1(r) = N_1/\gamma, \tag{9c}$$

where the renormalized value N_1/γ far away from the island edge is due to the fact that the average local monomer density is actually larger than the overall monomer density N_1 by a factor of $1/\gamma$.

Since the growth is isotropic, there is no angular dependence in the model and the general solution of Eqs. (8) satisfying the boundary condition (9c) at infinity is given by

$$n_1(r) = \begin{cases} N_1[\alpha^2/\gamma + aI_0(r/\xi_1) + bK_0(r/\xi_1)] \\ \quad \text{for } R_s < r \leqslant R_{ex} \\ N_1[1/\gamma + cK_0(r/\xi)] \quad \text{for } R_{ex} < r < \infty. \end{cases} \tag{10}$$

The coefficients a and b are determined by the boundary conditions (9a) and (9b),

$$a = \frac{1}{\gamma} \frac{\alpha^3(K_{1x}K_{0x1} - K_{1x}K_{0s1}) - \alpha^2 K_{0x}K_{1x1} + \alpha K_{1x}K_{0s1}}{K_{0x}(I_{1x1}K_{0s1} - K_{1x1}I_{0s1}) + \alpha K_{1x}(I_{0x1}K_{0s1} - K_{0x1}I_{0s1})}, \tag{11a}$$

$$b = -\frac{\alpha^2/\gamma + aI_{0s1}}{K_{0s1}}, \tag{11b}$$

where $K_{js1} = K_j(R_s/\xi_1)$, $K_{jx} = K_j(R_{ex}/\xi)$, $K_{jx1} = K_j(R_{ex}/\xi_1)$ (and similarly for I_{js1}, I_{jx}, and I_{jx1}), and $K_j, I_j, j \in \{0,1\}$ are the modified Bessel functions of order j.

Equating the *microscopic* flux of atoms near the island, $2\pi R_s D[dn_1/dr]_{r=R_s}$, to the corresponding *macroscopic* RE-like term $DN_1\tilde{\sigma}_s(A_V)$, one obtains an expression for the local capture number $\tilde{\sigma}_s(A_V)$,

$$\tilde{\sigma}_s(A_V) = \frac{2\pi R_s}{\xi_1}\left[aI_1\left(\frac{R_s}{\xi_1}\right) - bK_1\left(\frac{R_s}{\xi_1}\right)\right]. \tag{12}$$

Here the dependence of $\tilde{\sigma}_s$ on the Voronoi area A_V (or equivalently on the exclusion-zone area $A_{ex} = \eta A_V$) arises from the dependence of the coefficients a and b on the exclusion-zone radius $R_{ex} = \sqrt{\eta A_V/\pi}$.

A similar analysis can be carried out for the monomer capture number σ_1. However, since the monomers are mobile, in this case there is no ''exclusion'' zone, which implies that $R_{ex}=R_1$. In this limit, i.e., taking $R_s=R_1=R_{ex}$, Eqs. (11) and (12) lead to

$$\sigma_1=\frac{2\pi R_1}{\gamma\xi}\frac{K_1(R_1/\xi)}{K_0(R_1/\xi)}. \tag{13}$$

Apart from an extra factor of $1/\gamma$, which takes into account the enhancement of the local monomer density with increasing coverage, this expression is the same as previously obtained by Bales and Chrzan.[20]

Using Eq. (12), the size-dependent capture numbers σ_s are obtained by averaging the local capture numbers $\tilde{\sigma}_s(A_V)$ over the distribution of Voronoi areas. Defining $G_s(\theta;A_V)$ as the number density of Voronoi areas of size A_V surrounding an island of size s at coverage θ, we can write

$$\sigma_s(\theta)=\langle\tilde{\sigma}_s(A_V)\rangle_{G_s}\equiv\frac{\sum_{A_V}G_s(\theta;A_V)\tilde{\sigma}_s(A_V)}{\sum_{A_V}G_s(\theta;A_V)}$$

$$=\frac{1}{N_s}\sum_{A_V}G_s(\theta;A_V)\tilde{\sigma}_s(A_V), \tag{14}$$

where $\langle\cdots\rangle_{G_s}$ denotes an average with respect to the distribution $G_s(\theta;A_V)$.

The capture numbers σ_s have now been expressed in terms of the Voronoi-area distribution $G_s(\theta;A_V)$, the geometrical factors ρ and η, and the nucleation and screening lengths ξ_1 and ξ. The nucleation length ξ_1 can be determined using Eqs. (3) and (13), assuming ρ and ξ are known. Once the distributions $G_s(\theta;A_V)$ and the parameters ρ, η, and ξ are known, Eqs. (12), (13), and (14) can be solved in order to obtain the size- and coverage-dependent capture numbers σ_s. However, the local monomer density and capture numbers must satisfy self-consistency conditions that we discuss in the next section. Use of these self-consistency conditions allows the determination of two of the three parameters η, ρ, and ξ once the third is known.

C. Self-consistency conditions for monomer density and capture numbers

The parameters ρ and η are independent of the island size and Voronoi areas, and thus they can be determined using an approximation in which the Voronoi areas surrounding islands of size s are replaced by their average values. Denoting the average Voronoi area corresponding to an island of size s at a given coverage θ by A_s, this leads to the approximation $\sigma_s=\tilde{\sigma}_s(A_s)$. The definition (4) of the screening length ξ then leads to the capture number self-consistency condition,

$$2\sigma_1N_1+\sum_{s\geqslant 2}N_s\tilde{\sigma}_s(A_s)=1/\xi^2, \tag{15}$$

which corresponds to the requirement that the average ''screening length'' embodied in the rate equations is the same as that expressed by the diffusion equations.

If $n_1^t(A_s)$ denotes the total number of monomers in a Voronoi area of size A_s surrounding an island of size s, then the self-consistency condition for the monomer density corresponds to the requirement that the total monomer density in the Voronoi polygons must be equal to the average monomer density N_1, i.e.,

$$\sum_{s\geqslant 2}N_sn_1^t(A_s)=N_1. \tag{16}$$

In principle, Eqs. (15) and (16) can be solved at any given coverage θ for two of the three unknowns ξ, η, and ρ once the third is known and once the average Voronoi area A_s is known for all s. However, by carrying out detailed numerical comparisons we have found[42] that a mean-field approximation gives equally good results. This is not surprising, since the self-consistency conditions correspond to *average* quantities. This approximation allows us to ''precalculate'' the quantities ρ, η, ξ, and ξ_1 as a function of coverage before carrying out the numerical integration of the full island-density rate equations (1) and (2) coupled with the Voronoi-area rate equations (see below).

In this approximation, the island sizes s in Eqs. (15) and (16) are replaced by the average island size $S=(\theta-N_1)/N$, while the corresponding Voronoi areas are replaced by the average Voronoi area $A_{av}=1/N$. This leads to a very simple form for the capture number and monomer density self-consistency relations,

$$2\sigma_1N_1+N\tilde{\sigma}_S(A_{av})=1/\xi^2, \tag{17a}$$

$$N\int_{R_S}^{R_{av}}dr\ 2\pi rn_1(r)=N_1, \tag{17b}$$

where $R_S=\rho S^{1/d_f}$ and $R_{av}=\sqrt{1/(\pi N)}$.

Using Eq. (10) for the monomer density $n_1(r)$, the monomer-density self-consistency condition (17b) may be rewritten for the case $\eta\geqslant 1$ as

$$R_{av}^2(\alpha^2/\gamma-1)-R_S^2\alpha^2/\gamma-2R_S\xi_1(aI_{1S1}-bK_{1S1})$$
$$+2R_{av}\xi_1(aI_{1a1}-bK_{1a1})=0, \tag{18}$$

where $I_{1a1}=I_1(R_{av}/\xi_1)$, $K_{1a1}=K_1(R_{av}/\xi_1)$, and the coefficients a and b are given by Eq. (11) with $R_{ex}=\sqrt{\eta}R_{av}$. A similar expression can be written for the monomer-density self-consistency condition for the case $\eta\leqslant 1$.

In the case of extended islands, the geometrical parameter ρ was assumed to be independent of coverage, and its value $\rho\simeq 0.3$ was selected such that numerical integration of a mean-field form of the island-density rate equations (1) and (2)—corresponding to replacing A_V in Eq. (12) with $A_{av}=1/N$—led to good agreement with Monte Carlo results for the average monomer and island densities N_1 and N. Although the value $\rho\simeq 0.3$ is somewhat smaller than expected (for circular islands the value of ρ would be $1/\sqrt{\pi}\simeq 0.6$), the same value works for all values of R while variations of

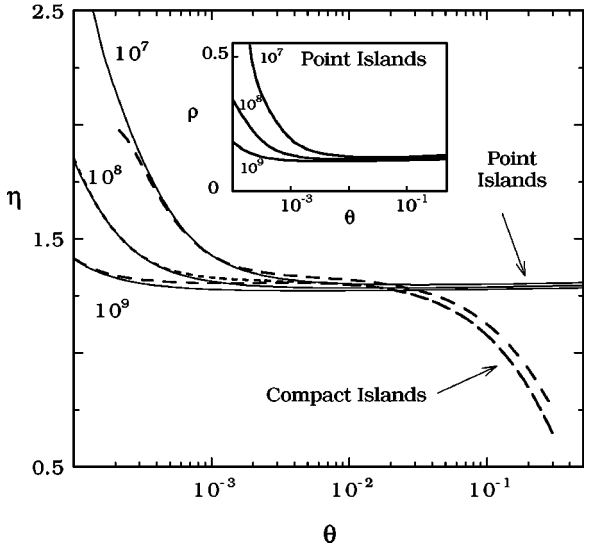

FIG. 2. Coverage-dependence of η obtained from Eqs. (17) for point islands (solid lines) and compact islands (dashed lines) for $R_h = 10^7 - 10^9$. Inset shows corresponding coverage dependence of ρ for point islands.

about 20% in ρ lead to significant deviations from the Monte Carlo calculated densities N and N_1. The two remaining variables η and ξ were then determined by simultaneously solving the two self-consistency conditions (17) as a function of coverage.

In the case of point islands a slight variation of this method was found to lead to better results. In this case there is no explicit s dependence in $\tilde{\sigma}_s$ since $R_s = \rho$ for all s. Thus, Eq. (17a) may be rewritten as

$$1/\xi_1^2 + N\tilde{\sigma}(A_{av}) = 1/\xi^2 \tag{19}$$

without any additional assumption of an average island size S. In this case, a self-consistent RE approach similar to that used in Ref. 20 for compact islands was first used in order to obtain the coverage-dependent lengths $\xi_1(\theta)$ and $\xi(\theta)$ for point islands. Equations (17b) and (19) were then simultaneously solved for $\rho(\theta)$ and $\eta(\theta)$.

Figure 2 shows the resulting coverage dependence of η for both point and compact islands. As expected, similar values of η are obtained at low coverage for both point and compact islands. In particular, we find $\eta \gg 1$ in the nucleation regime corresponding to $\theta < \theta_x$, where θ_x [defined by $N_1(\theta_x) = N(\theta_x)$] corresponds to the crossover from nucleation to aggregation. However, for $\theta \gg \theta_x$, η quickly approaches a constant value for point islands, which is somewhat above 1 and is slightly dependent on $R_h = D_h/F$. In contrast, for extended islands η continues to decrease in the coverage range where the spatial extent of an island is significant, and it eventually becomes smaller than 1 at coverages higher than $\theta \approx 0.2$. This may be considered as a natural limit of our method since in that range coalescence effects, which are not included in our rate equations, become significant. It is interesting to note, however, that this decrease actually correctly describes the qualitative behavior of η in the presence of coalescence.

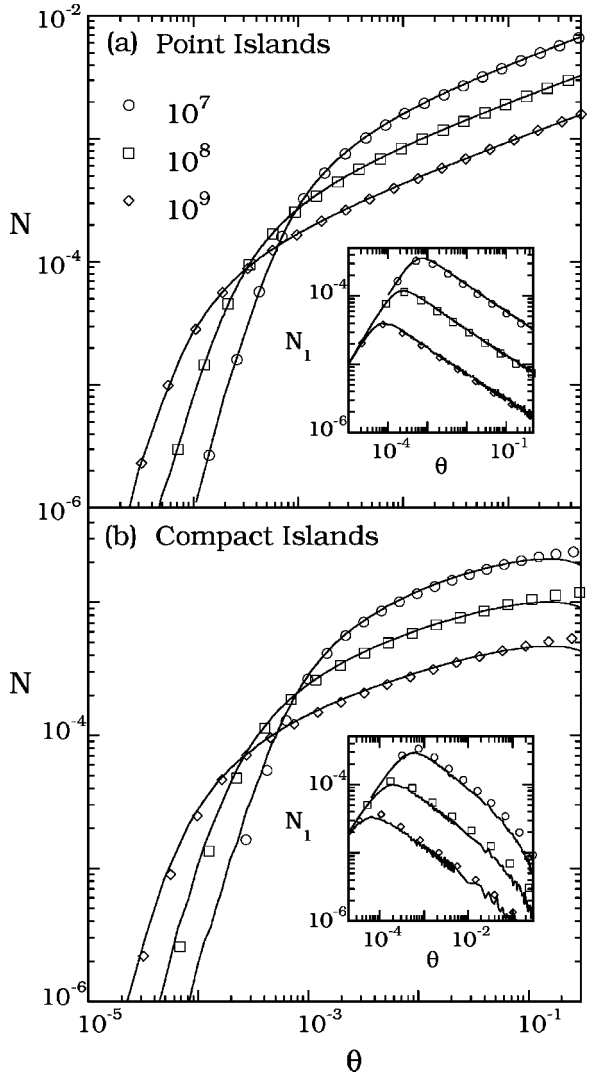

FIG. 3. Island density N and monomer density N_1 as a function of coverage θ for $R_h = 10^7 - 10^9$ obtained from RE's (symbols) and KMC (solid lines) for (a) point and (b) compact islands.

The inset in Fig. 2 shows our results for $\rho(\theta)$ for the case of point islands. As expected, $\rho(\theta)$ is almost constant and independent of $R_h = D_h/F$ for $\theta \geq 0.01$, and asymptotically (i.e., in the limit of large R_h) approaches a constant value over the entire coverage range. Accordingly, in our calculation of the island-capture numbers and size distributions for point islands, we have approximated $\rho(\theta)$ by the constant value $\rho \simeq 0.12$ at all coverages. It is not surprising that this value is significantly smaller than the value $\rho \simeq 0.3$ used for extended islands, since for point islands, monomers can only attach by landing on the site occupied by another island or monomer, and not by nearest-neighbor attachment.

Figure 3 shows the resulting average island and monomer densities N and N_1 obtained using the island-density rate equations (1) and (2), as discussed above, along with the corresponding KMC simulation results. As can be seen, there is excellent agreement between the RE predictions and the simulation results for these average quantities at all coverages in the precoalescence regime. Thus, the coverage-

dependent factors ρ and η and the screening and nucleation lengths ξ and ξ_1 have been calculated using the mean-field self-consistency conditions. The only quantity left unknown is the distribution of Voronoi areas.

III. VORONOI-AREA-DISTRIBUTION EVOLUTION EQUATIONS

To obtain the capture numbers and the island-size distribution, one has to consider the dependence of the Voronoi-area distribution $G_s(\theta;A)$ on the island size s. Taking into account the change in the areas by nucleation and aggregation of islands, and ignoring for the moment the breakup of Voronoi areas when new islands are nucleated, one can write a general set of evolution equations for the functions $G_s(\theta;A)$ in the following form:

$$\frac{dG_2(\theta;A)}{d\theta}=(dN/d\theta)\,\delta(A-A_{av})-RN_1\tilde{\sigma}_2(A)G_2(\theta;A), \tag{20}$$

$$\frac{dG_s(\theta;A)}{d\theta}=RN_1[\tilde{\sigma}_{s-1}(A)G_{s-1}(\theta;A)-\tilde{\sigma}_s(A)G_s(\theta;A)] \quad (s\geqslant 3), \tag{21}$$

where $\tilde{\sigma}_s(A)$ is the local capture number as given by Eq. (12). The first term on the right side of Eq. (20) corresponds to nucleation of dimers while the remaining terms in Eqs. (20) and (21) correspond to growth of islands via aggregation. We note that in these equations it has been assumed that the Voronoi areas around the (new) dimers nucleated at coverage θ are equal to the average Voronoi area at that coverage, $A_{av}=1/N$, and for simplicity the ''source'' term in Eq. (20) has been assumed to take the form of a delta function.

As already noted, the breakup of larger areas due to nucleation has been neglected in Eq. (21). However, we will account for it through a uniform rescaling that will be justified *a posteriori*. The effects of direct impingement of atoms on islands have also been neglected in Eqs. (20) and (21) since they are very small except for the case of extended islands at high coverages. However, direct impingement is still taken into account in the full rate equations (1) and (2).

Defining θ_A through the condition $A=1/N(\theta_A)$, the nucleation term in Eq. (20) may be rewritten as $B_A\delta(\theta-\theta_A)$, with $B_A=1/A^2$. Accordingly, Eq. (20) may be rewritten in the form

$$\frac{dG_2(\theta;A)}{d\theta}=-RN_1\tilde{\sigma}_2(A)G_2(\theta;A)+B_A\delta(\theta-\theta_A). \tag{22}$$

We note that the initial conditions (for a given A) for the functions $G_s(\theta;A)$ are determined by $G_s(\theta;A)\equiv 0$ for all s for $\theta<\theta_A$. Since the solution of Eqs. (21) and (22) is somewhat dependent on the particular growth model (point or extended islands), we discuss the two cases separately.

A. Voronoi-area distributions for point islands

The point-island model is special because for this model the local capture numbers do not depend explicitly on the island size s. This allows an exact solution of the Voronoi-area evolution equations (21) and (22). Changing the coverage variable from θ to

$$x_A=\int_{\theta_A}^{\theta}RN_1(\phi)\tilde{\sigma}(A)\,d\phi, \tag{23}$$

where $\tilde{\sigma}(A)$ is the local capture number for point islands, leads to the following form of the Voronoi-area evolution equations:

$$\frac{dG_2(x_A;A)}{dx_A}=-G_2(x_A;A)+B_A\delta(x_A), \tag{24}$$

$$\frac{dG_s(x_A;A)}{dx_A}=G_{s-1}(x_A;A)-G_s(x_A;A) \quad (s\geqslant 3). \tag{25}$$

The solution of Eq. (24) is $G_2(x_A;A)=B_Ae^{-x_A}H(x_A)$, where $H(z)$ is the step function $[H(z)=1,z\geqslant 0;H(z)=0,z<0]$. It can also be shown[32] that the general solution for the Voronoi-area distribution G_s for $s\geqslant 2$ is

$$G_s(x_A;A)=B_Ax_A^{s-2}e^{-x_A}/(s-2)!. \tag{26}$$

At coverages beyond the nucleation regime, both x_A and the average Voronoi area A_{av} are typically large. Thus, Eq. (26) corresponds to a sharply peaked distribution as a function of A, and the peak position $\hat{A}_s$ satisfies[43]

$$x_{\hat{A}_s}=s-2. \tag{27}$$

Therefore, keeping only the dominant terms in the sums, the average Voronoi area A_s corresponding to an island of size s and the corresponding capture numbers σ_s satisfy

$$A_s\equiv\frac{\sum_A AG_s(x_A;A)}{\sum_A G_s(x_A;A)}\simeq\hat{A}_s, \tag{28}$$

$$\sigma_s\equiv\frac{\sum_A\tilde{\sigma}_s(A)G_s(x_A;A)}{\sum_A G_s(x_A;A)}\simeq\tilde{\sigma}_s(\hat{A}_s). \tag{29}$$

However, since Eqs. (20) and (21) do not include the effects of the area breakup due to nucleation, the average areas calculated using Eq. (27) are expected to be larger than the correct values. To account for this, the areas should be rescaled to the correct average Voronoi area, $A_{av}=1/N$. The correct capture numbers σ_s are then given by

$$\sigma_s=\tilde{\sigma}_s(A_s'), \quad \text{where} \quad A_s'=\frac{A_s}{\sum_s N_sA_s}, \tag{30}$$

where the local capture number $\tilde{\sigma}_s(A)$ is given by Eq. (12). Therefore, the calculation of the size-dependent capture numbers σ_s has been reduced to solving Eq. (27) for the peak position $\hat{A}_s$ and then rescaling using Eq. (30) to obtain the rescaled capture areas A_s'. Once the capture numbers σ_s are known at each step, the rate equations (1) and (2) can then be integrated to obtain the island-size distributions.

It is interesting to note that the variable x_A given in Eq. (23) has a simple physical interpretation, which also implies a simple physical interpretation for the peak condition (27). Since the quantity $RN_1(\phi)\tilde{\sigma}(A)$ is the average growth rate at coverage ϕ of a point island surrounded by a capture zone of area A, the coverage variable $x_A=\int_{\theta_A}^{\theta} d\phi\ RN_1(\phi)\tilde{\sigma}(A)$ is the average number of particles gained by a point island with Voronoi area A from the coverage θ_A at which it is nucleated up to the current coverage θ. Thus the peak condition $x_{\hat{A}_s}=s-2$ given by Eq. (27) may be viewed as stating that the peak of the Voronoi-area distribution $G_s(A)$ corresponds to islands whose Voronoi area is such that they have on average gained $s-2$ particles since their nucleation as dimers, assuming that their capture-zone area did not change since they were nucleated.

B. Voronoi-area distributions for extended islands

In the case of extended islands the Voronoi-area evolution equations (21) cannot be solved analytically due to the explicit s dependence of the local capture numbers $\tilde{\sigma}_s(A)$. However, using the approximation $\tilde{\sigma}_s(A)\simeq\tilde{\sigma}_S(A)$ (where S is the average island size) leads to a set of equations that can be solved analytically. This approximation is expected to have only a weak effect on the final island-size distributions $N_s(\theta)$ because it retains the dominant effect, i.e., that of an exclusion zone A_{ex}, which depends on the island size s. Furthermore, the correct expression for $\sigma_s(A_s)$ will be retained in the rate equations (1) and (2).

Using this approximation, the Voronoi-area evolution equations become

$$\frac{dG_2(\theta;A)}{d\theta}=(dN/d\theta)\,\delta(A-A_{av})-RN_1\tilde{\sigma}_S(A)G_2(\theta;A), \tag{31}$$

$$\frac{dG_s(\theta;A)}{d\theta}=RN_1\tilde{\sigma}_S(A)[G_{s-1}(\theta;A)-G_s(\theta;A)] \quad (s\geqslant 3). \tag{32}$$

One can again transform to new variables,

$$x_A=\int_{\theta_A}^{\theta} RN_1(\phi)\tilde{\sigma}_S(A)\,d\phi \tag{33}$$

to obtain the evolution equations

$$\frac{dG_2(x_A;A)}{dx_A}=-G_2(x_A;A)+B_A\delta(x_A), \tag{34}$$

$$\frac{dG_s(x_A;A)}{dx_A}=G_{s-1}(x_A;A)-G_s(x_A;A) \quad (s\geqslant 3) \tag{35}$$

for the Voronoi-area distributions. The solution is again given by

$$G_s(A)=B_A x_A^{s-2}e^{-x_A}/(s-2)!, \tag{36}$$

with the peak of the distribution (for a given s) corresponding to $\hat{A}_s$ determined by

$$x_{\hat{A}_s}=s-2, \tag{37}$$

and from Eq. (28) the average Voronoi area is $A_s\simeq\hat{A}_s$.

As before, the effects of the breakup of Voronoi areas due to nucleation will be included through a rescaling of the areas to the correct average value $A_{av}=1/N$. However, due to the existence of a spatially extended island inside the Voronoi area, one should consider the rescaling due to breakup to apply only to the area at the exterior of the island, rather than to the whole area. Therefore, one obtains for the rescaling factor, the expression

$$f=\frac{\gamma}{\sum_s A_s N_s+\gamma-1}. \tag{38}$$

We note that for extended islands it is reasonable to define the Voronoi polygon as passing through points halfway from the *edges* of the islands rather then halfway from the centers.[44] Ignoring correlations between the size of an island and the size of its neighbors, the radius of the rescaled Voronoi polygon should then include an additional correction, $R_{corr}=\rho(s^{1/d_f}-S^{1/d_f})/2$. This leads to the corrected Voronoi area

$$A_s'=\pi(\sqrt{fA_s/\pi}+R_{corr})^2, \tag{39}$$

and the capture numbers are given by

$$\sigma_s=\tilde{\sigma}_s(A_s'). \tag{40}$$

Therefore, the calculation of the coverage-dependent capture numbers σ_s for extended islands has been reduced to solving Eqs. (33) and (37), and the full rate equations (1) and (2) can be integrated to find the island-size distributions.

C. Summary

Before presenting our results, we now summarize the key points and physical assumptions used in our approach with an emphasis on the case of extended islands. The environment of an island is modeled as consisting of an inner ''exclusion'' zone in which only monomers can be found, which is surrounded by an outer ''smeared'' zone consisting of both monomers and islands, while a circular approximation for the island and exclusion zone areas is used. In order to connect the island radius R_s to the island size s as well as the radius of the exclusion zone R_{ex} to the Voronoi cell area A_V, two geometrical parameters ρ and η were introduced.

By combining the linearized diffusion equation (6) satisfied by the local monomer density surrounding an island with the contracted rate equation (5) for the average monomer density, and solving the resulting quasistatic monomer-diffusion equation (8) with the appropriate boundary conditions, a self-consistent expression (12) for the local capture number in terms of the island size and exclusion-zone area was derived. The geometrical parameter $\eta(\theta)$ and the capture length $\xi(\theta)$ are precalculated as a function of coverage using the mean-field monomer density and capture-number self-consistency conditions (17), while the geometrical parameter ρ is determined by the requirement of reproducing the KMC and/or mean-field RE results for the total island and monomer densities.

In order to find the distribution of exclusion zones, a set of Voronoi-area evolution equations is used, which takes into account the change in the areas by nucleation and aggregation of islands, while the effects of fragmentation are included through a uniform rescaling of the areas. By introducing a change of variables [and using an additional approximation for the case of extended islands in which the local capture number $\tilde{\sigma}_s(A)$ is approximated by $\tilde{\sigma}_S(A)$] these equations can be solved in closed form. For large s (corresponding to large values of $R_h = D_h/F$) the solution in Eq. (36) is a sharply peaked distribution as a function of the Voronoi area A, and the peak position $\hat{A}_s$ satisfies the condition $x_{\hat{A}_s} = s - 2$ given by Eq. (37). Thus, the most important and time-consuming aspect of our approach involves solving Eq. (37) numerically for each value of s at each integration step. In calculating the coverage variable x_A for each value of A needed in the numerical routine (we have used Ridders's method), Eq. (12) is used for the local capture number $\tilde{\sigma}_S(A)$, which enters in Eq. (33). We note that calculating x_A using Eq. (33) also requires knowing $N_1(\phi)$, $\xi_1(\phi)$, $\xi(\phi)$, and $S(\phi)$ [or $N(\phi)$] for all coverages ϕ up to the present value θ. While in principle these values can be calculated and stored during the integration, for convenience they are precalculated using a mean-field approach as described in Sec. II C (specific values are obtained via interpolation). Once the values $\hat{A}_s$ have been calculated for all s, they are rescaled following Eqs. (38) and (39) to obtain the areas A'_s. As described in Eq. (40), A'_s is then used in Eq. (12) to obtain the capture numbers σ_s. The resulting capture numbers $\sigma_s(\theta)$ are then used to advance the full rate equations (1) and (2) in order to obtain the island-size distribution.

IV. RESULTS

Using the methods described in the previous sections, the island-density rate equations (1) and (2) were numerically integrated along with the Voronoi-area evolution equations in order to obtain the size- and coverage-dependent capture numbers $\sigma_s(\theta)$ as well as the scaled island-density distributions $f(s/S) = (S^2/\theta)N_s(\theta)$. The rate equations were numerically integrated starting at very low coverage $\theta_0 \ll \theta_x$ with initial conditions $N_1(\theta_0) = \theta_0$ and $N_s(\theta_0) = 0$ for $s \geq 2$. At low coverage, for which both the average island size S and typical values of x_A are small, the average capture number $\sigma_{av} = (1/\xi^2 - 1/\xi_1^2)/N$ was used in the island-density rate equations. However, at coverages (just beyond θ_x) such that the average island size S is sufficiently large (we chose as criterion $S \geq 10$) and the peak in the Voronoi-area distribution $G_s(\theta;A)$ is well defined, the appropriate Voronoi-area evolution equation results for σ_s, i.e., Eq. (30) for point islands and Eq. (40) for extended islands, were used.

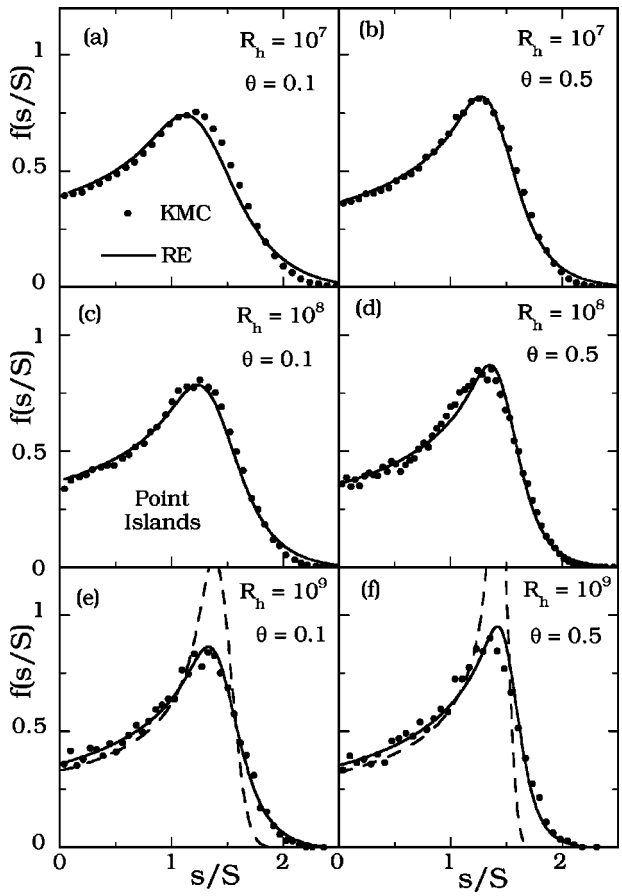

FIG. 4. Scaled island-size distribution $f(s/S)$ for point islands calculated using RE's (solid lines), along with corresponding KMC results (symbols) and MF theory (dashed lines) for $R_h = 10^7 - 10^9$.

A. Point islands

Figure 4 shows our rate-equation results for the scaled island-size distribution for point islands (solid lines) in the aggregation regime ($\theta = 0.1$–0.5) for $R_h = 10^7 - 10^9$. Also shown are the corresponding KMC simulation results (symbols) and, for comparison, mean-field (MF) RE results ($R_h = 10^9$) obtained using the approximation $\sigma_s = \sigma_{av}$ (dashed lines). As can be seen, there is excellent agreement between the RE predictions obtained using the Voronoi-area evolution equations and the corresponding kinetic Monte Carlo simulation results. In contrast, the mean-field results are much more sharply peaked and appear to be approaching the (divergent) asymptotic form[16,28,30] $f_{MF}(u) = (1/3)(1 - 2u/3)^{-1/2}$.

The good agreement between the results obtained using the Voronoi-area evolution equations and the kinetic Monte

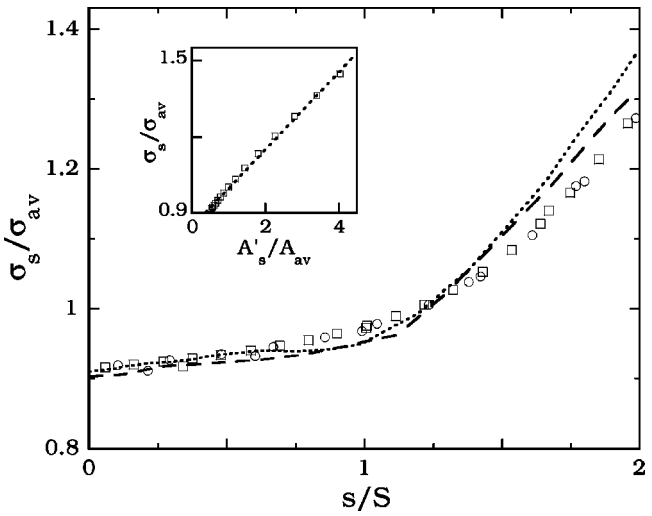

FIG. 5. RE results (symbols) for scaled capture-number distributions σ_s/σ_{av} for point islands at coverages $\theta=0.1$ (circles) and $\theta=0.5$ (squares) for $R_h=10^8$ and 10^9. Lines are KMC results from Ref. 30 at $\theta=0.2$ for $R_h=10^8$ (dashed) and 10^9 (dotted). Inset shows RE results (symbols) for dependence of σ_s/σ_{av} on scaled Voronoi area at $R_h=10^9$, $\theta=0.5$.

Carlo simulations is due to the inclusion of explicit correlations, which are not taken into account in the mean-field calculations. We note, however, that for $\theta=0.5$ and high D/F the predicted distributions are shifted slightly to the right of the simulation results. This is most likely due to the fact that the uniform rescaling of the Voronoi areas does not exactly take into account the effects of breakup of exclusion zones due to nucleation.

Figure 5 shows the corresponding results for the scaled capture number distribution σ_s/σ_{av} as a function of the scaled island size for $R_h=10^8$ and 10^9. As can be seen, the scaled capture-number distribution is essentially independent of coverage and R_h, but depends strongly on the scaled island size for $s/S>1$. Also shown (dashed lines) are KMC simulation results at $\theta=0.2$ for $R_h=10^8-10^9$ from Ref. 30. As can be seen, there is good agreement with the simulations, although for large s/S and R_h the RE results are slightly below the KMC results.

The strong island-size dependence of the scaled capture numbers shown in Fig. 5 is due to the fact that the average Voronoi areas also depend strongly on the island size. As shown by the inset in Fig. 5, the capture numbers are to a good approximation linearly dependent on the Voronoi areas,

$$\sigma_s/\sigma_{av}=a_0+a_1(A_s'/A_{av}). \tag{41}$$

The linear fit shown in the inset (dotted line) gives[46] $a_0\simeq 0.85$, $a_1\simeq 0.15$. These values are significantly different from the values $a_0\simeq 0.3$, $a_1\simeq 0.7$ obtained from simulations of a two-dimensional point-island model in Ref. 30. The difference in a_0 and a_1 indicates a possible difference between the Voronoi areas obtained in our area-evolution plus rate-equation results and those obtained in the simulations.[44]

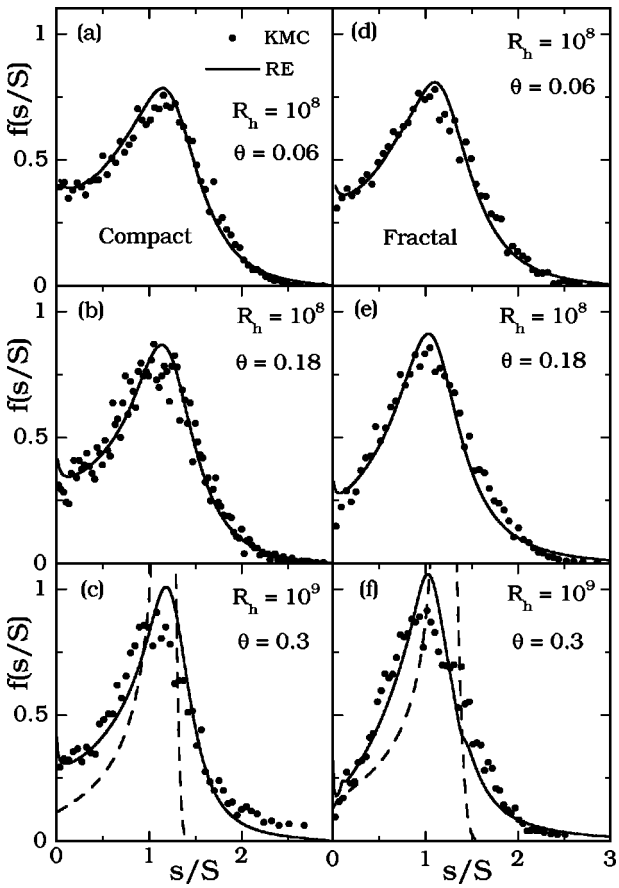

FIG. 6. Scaled island-size distribution $f(s/S)$ for (a)–(c) compact islands ($d_f=2$) and (d)–(f) fractal islands ($d_f=1.72$) for $R_h=10^8-10^9$ and $\theta=0.06-0.3$, obtained from RE's (lines) and KMC (symbols), along with MF theory (dashed lines).

However, as already noted, this difference does not appear to have a significant effect on the scaled capture numbers σ_s/σ_{av}.

B. Extended islands

Figure 6 shows our rate-equation results for the scaled island-size distribution for both compact islands ($d_f=2$) and fractal islands ($d_f=1.72$) in the aggregation regime ($\theta=0.06$–0.3) for $R_h=10^8$ and 10^9, along with the corresponding KMC simulation results and mean-field predictions at $R_h=10^9$ (dashed lines). Similar results have also been obtained for $R_h=10^7$ (not shown). As can be seen, the predicted island-size distributions are in good agreement with the simulation results, while the mean-field distributions are much too sharply peaked and diverge rapidly with increasing coverage. In addition, we note that the predicted position of the peak in the size distribution is almost coverage independent for compact islands, while for fractal islands it is shifting slightly to the left with increasing coverage, in very good agreement with the behavior shown by the KMC results. However, for both compact and fractal islands there is a small ''overshooting'' of the peak value, which increases with coverage and/or R_h. This is most probably due to the use of the mean-field approximation $s=S$ in the Voronoi-area evolution equations.[45]

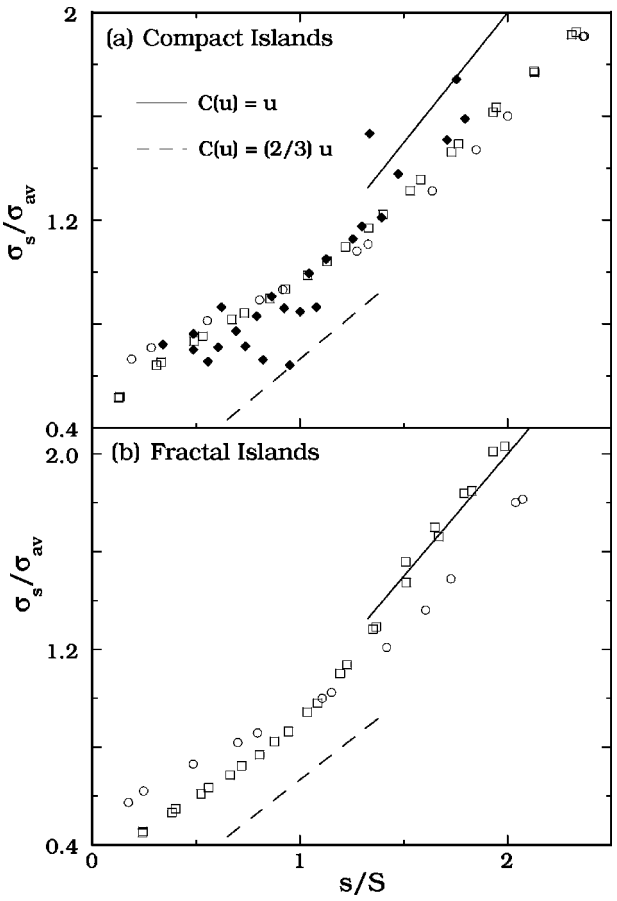

FIG. 7. RE results for scaled capture-number distributions for (a) compact and (b) fractal islands for $R_h = 10^8$ and 10^9 at $\theta = 0.06$ (open circles) and 0.3 (open squares), along with experimental results (filled symbols) at $\theta = 0.23$ from Ref. 31.

Another important difference between compact and fractal islands is the behavior of the size distribution at small s/S values. While for both point and compact islands $f(0)$ appears to approach a common limiting value $f(0) \simeq 1/3$ in agreement with the MF rate-equation prediction[16,28,30] (see Figs. 4 and 6), for fractal islands our rate-equation results correctly follow the decrease of $f(0)$ with increasing coverage,[47] as shown in Fig. 6. This indicates that the decrease in $f(0)$ with increasing coverage is not due to coalescence, since coalescence is not taken into account in the island-density rate equations or Voronoi-area evolution equations, but is most likely due to the increase in the average capture number σ_{av} with coverage for fractal islands.

The difference in the behavior of $f(0)$ for compact and fractal islands is somewhat surprising, since the only change in the rate equations from compact to fractal islands is the value of the fractal dimension d_f. In order to understand this result, as well as the good predictions for the island size distributions and for the peak position, we have analyzed the behavior of the capture numbers for each case. Figure 7(a) shows the scaled capture-number distribution σ_s/σ_{av} for compact islands as a function of s/S for $R_h = 10^8$–10^9 and $\theta = 0.06$–0.3 along with the *experimentally* measured capture-number distribution for Cu/Co on Ru(0001) from Ref. 31. The RE results show excellent scaling with both R_h and coverage, and there is good agreement within statistical fluctuations with the experimental data. Also shown in Fig. 7(a) are lines corresponding to the asymptotic forms[31] $\sigma_s/\sigma_{av} = zs/S$, where $z = 2/3$ for point islands and $z = 1$ (with logarithmic corrections) for compact islands. Both the experimental and the RE results lie between these two lines, thus showing an effective value of z smaller than 1, but greater than 2/3, in agreement with the experimental results of Ref. 31.

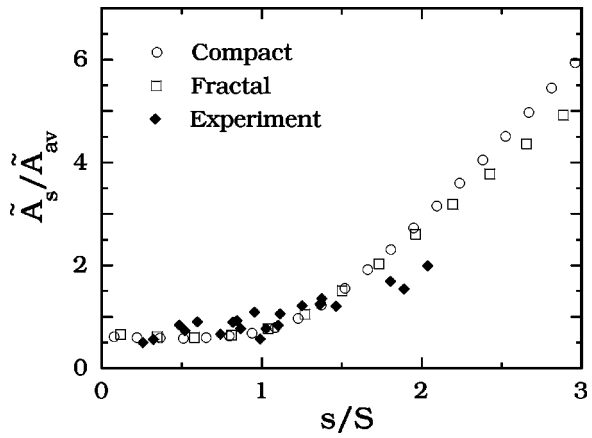

FIG. 8. RE results for scaled average capture zone $\tilde{A}_s/\tilde{A}_{av}$ for compact (open circles) and fractal (open squares) islands ($R_h = 10^9, \theta = 0.18$) along with experimental results (filled symbols) at $\theta = 0.23$ from Ref. 31.

In contrast to the results for compact islands, for fractal islands the scaled capture-number distribution is independent of R_h, but depends on coverage, as shown in Fig. 7(b). With increasing coverage the distribution σ_s/σ_{av} "rotates" counterclockwise around the point $s/S = 1$, and this may explain the differences in the island-size distributions. The decrease in the scaled capture numbers for $s/S < 1$ with increasing coverage (and the corresponding increase for $s/S > 1$) is consistent with both the decrease of $f(0)$ and the shift of the fractal-island size-distribution peak toward $s/S = 1$, and also explains the incomplete scaling shown by the fractal island-size distributions. It can also be seen that, in contrast to the compact case, the asymptotic behavior of the scaled capture number at large s seems to be well described by the asymptotic value $z = 1$.

Figure 8 shows the scaled "capture zone" $\tilde{A}_s/\tilde{A}_{av}$ for both compact and fractal islands as a function of the scaled island size. We note here that in agreement with Ref. 31, we have defined $\tilde{A}_s = A_s' - s$, thus $\tilde{A}_{av} = \gamma A_{av}$, as corresponding to the part of the capture zone *outside* the island (for a very detailed discussion of this point see Ref. 44). Also shown in Fig. 8 are the experimental results at $\theta = 0.23$ for Cu/Co on Ru(0001) from Ref. 31. Again, there is good agreement between the predicted capture zones and the experimental results for $s/S < 1.75$. However, for $s/S > 1.75$, the RE predictions are somewhat above the experimentally measured values. This may be due in part to insufficient statistics in the experiment for large island sizes or to a slight breakdown of the uniform rescaling assumption used in our RE's. In any

case, as already noted these differences have little effect on the island-size distributions since in that range the island density is already very small and decreasing, as can be seen from Fig. 6.

Finally, we briefly discuss and present results for the scaled Voronoi-area distribution $g(A/A_{av})=(1/N)\Sigma_{s\geqslant 2}G_s(\theta;A)$, which may be obtained using our approach. While the uniform rescaling of the Voronoi areas appears to be sufficient to obtain good results for the capture numbers and island densities, a more complicated rescaling is necessary in order to obtain the Voronoi-area distribution $G(A)=\Sigma_{s\geqslant 2}G_s(\theta;A)$. The reason is easy to understand: rescaling the areas shifts the distribution and thus corrects the position of the peak, but leaves the amplitudes unchanged. Proper normalization of the Voronoi-area distributions $G_s(\theta;A)$ requires that they satisfy the condition $\int_0^\infty dA\, G_s(\theta;A)=N_s$ while the overall Voronoi-area distribution $G(A)$ must satisfy $\int_0^\infty dA\, G(A)=N$. While the latter normalization condition is automatically satisfied,[48] since the correct nucleation rate is included in the Voronoi-area evolution equations, the ''individual'' normalization conditions on the $G_s(\theta;A)$ as given by Eq. (36) are not, since the area rescaling is only carried out at the end of the calculation, rather than continuously during the integration involved in x_A.

While it is possible to rescale the $G_s(\theta;A)$ in Eq. (36) in order to obtain a prediction for the Voronoi-area distribution $G(A)$, calculation of the correct normalization factors (which involve integrals of the form $\int_0^\infty dA\, B_A x_A^{s-2} e^{-x_A}$) is rather tedious. Fortunately, a very simple approximation is possible. Since the distributions $G_s(\theta;A)$ given by Eq. (36) are sharply peaked around the rescaled areas A_s', it is reasonable to replace them, in a ''zeroth order'' approximation, by δ functions. Taking into account the proper normalization, we obtain

$$G_s(\theta;A)=N_s\delta(A-A_s'), \tag{42}$$

where A_s' is the rescaled peak area obtained from the Voronoi-area evolution equations [see Eq. (39)], while N_s are the island densities obtained from our island-density rate equations.

With this approximation, the Voronoi-area distribution $G(A)$ [which implicitly satisfies the correct normalization $\int_0^\infty dA G(\theta;A)=N(\theta)$], may be written as

$$G(\theta;A)=\sum_s N_s\delta(A-A_s'), \tag{43}$$

and thus the scaled Voronoi distribution $g(A/A_{av})$ is

$$g(A/A_{av})=\sum_s (N_s/N)\,\delta(A-A_s'). \tag{44}$$

Figure 9 shows results for the scaled Voronoi-area distribution $g(A/A_{av})$, Eq. (44), for compact islands ($R_h=10^8, \theta=0.18$) along with kinetic Monte Carlo simulation results ($R_h=4\times10^6, \theta=0.1-0.3$) from Ref. 25. As expected, the peak position is correctly predicted although the peak height is somewhat lower than obtained in simulations. The corresponding RE results for the point-island distribution (not shown) are similar, but the peak of the point-island distribution is shifted slightly to the right (compared to the compact-island case), consistent with KMC results obtained for circular islands at low coverage.[44] However, in both cases the tails of the predicted distributions are much wider than in the simulations and the RE results exhibit also a sharp cutoff for small A/A_{av}, in contrast to the smooth approach to zero of the simulation results. These discrepancies are the result of the neglect of the nonlinearity of the fragmentation process, which favors the breakup of large areas over small areas, and which can lead to the formation of small Voronoi areas with a nonvanishing probability. Overall, the qualitative agreement with the KMC results shown by the very simple approximate form Eq. (44) is surprisingly good, but it is clear that if quantitative predictions for the area distributions are needed, then the breakup should be accounted for in detail in the area evolution equations.

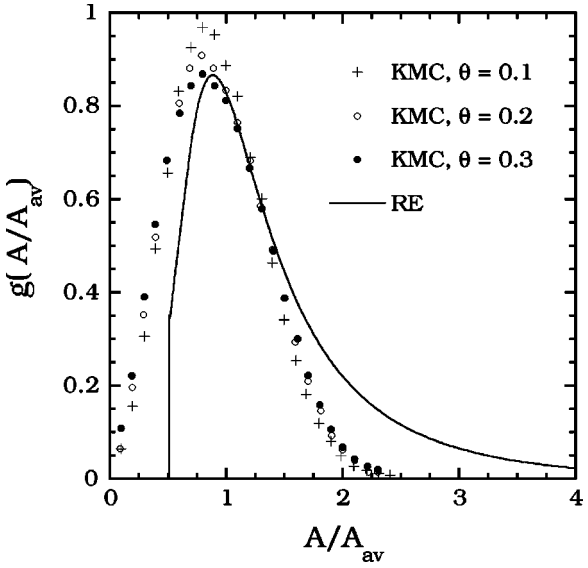

FIG. 9. Scaled Voronoi-area distribution $g(A/A_{av})$ obtained from Eq. (44) for compact islands (solid line) at $\theta=0.18$ for $R_h=10^8$, along with KMC results (symbols) for compact islands from Ref. 25 ($R_h=4\times10^6, \theta=0.1-0.3$.)

V. DISCUSSION

We have developed a self-consistent rate-equation approach to two-dimensional irreversible submonolayer growth in which the existence of a denuded (''capture'') zone with a fluctuating area around every island and the correlations between the size of the island and the corresponding average capture zone are explicitly taken into account. To obtain the capture numbers and the island size distribution, we have proposed a general set of evolution equations for the Voronoi-area distributions, which takes into account the change in the areas by nucleation and aggregation of islands, while the effects of fragmentation have been included through a uniform rescaling of the average Voronoi areas. This second set of equations has been solved analytically and

the solution has been used to self-consistently determine the size- and coverage-dependent capture numbers $\sigma_s(\theta)$. The resulting scaled island-size distributions were found to be in excellent agreement with KMC simulations, although a small ''overshooting'' of the peak value was noted for extended islands. In addition, our results were shown to accurately predict the dependence of the scaled island-size distribution on the island morphology as well as on the coverage and deposition rate. The island-size dependence of the capture numbers was also found to be in good agreement with simulation[30] and experimental[31] results.

We note that in previous work by Blackman and Mulheran[24] reasonably accurate asymptotic island-size distributions have been obtained in one dimension,[24] by using Monte Carlo simulation results for the scaled-gap distribution coupled with rate equations and assuming scaling. More recently, Mulheran and Robbie[25] have carried out a numerical calculation of both the asymptotic scaled Voronoi-area distribution $G(s/S;A/\langle A\rangle)$ and the asymptotic scaled island-size distribution $f(s/S)$ for compact islands in two-dimensions by assuming scaling as well as a linear relation between the Voronoi area and the island capture number.[25] In contrast, our method involves a fully self-consistent calculation of the coverage-dependent capture numbers $\sigma_s(\theta)$ without any assumptions regarding the relation between the island capture number and the capture-zone area. In addition, scaling of the island-size and capture-number distributions was not assumed. In this connection we note that in previous work[25,44] it has been pointed out that for irreversible growth the actual scaling is only approximate. Since we do not assume exact scaling (for a general discussion see Ref. 49), we are able to reproduce this approximate scaling including the coverage dependence of the scaled island-size distribution, as well as the dependence on the island morphology and R_h. As a result, our method leads to a self-consistent prediction for the evolution of the scaled capture-number and island-size distributions with coverage, which is in good agreement with both simulations and experiments.

Finally, we note that it should be possible to extend the coupled-evolution-equation method presented here to the case of reversible growth, in order to predict the scaled island-size distribution as a function of the critical island size i. For the case $i>1$, one may simply replace the equation for $G_2(\theta;A)$ with the corresponding equation for $G_{i+1}(\theta;A)$ while the Voronoi-area evolution equations for higher island sizes $s>i+1$ will remain the same. A self-consistent mean-field approach (see Refs. 21,33) can be used to obtain the nucleation rate $dN/d\theta$, as well as the densities and capture numbers of islands smaller than or equal to the critical island size. As a result, the quasistatic monomer diffusion equation inside the exclusion zone (Eq. 8) and all other expressions for the monomer density and capture numbers will remain the same, except that the monomer nucleation length ξ_1 should be replaced by the exclusion-zone capture length ξ_i, where $1/\xi_i^2=2\sigma_1 N_1+\Sigma_{2\leqslant s\leqslant i}\sigma_s N_s$. The basic idea of coupled evolution of the capture zones and densities included in the present approach may also prove useful in the rate-equation modeling of a variety of other problems involving growth by diffusion and aggregation, such as heteroepitaxial growth and Ostwald ripening.

ACKNOWLEDGMENT

This research was supported by a grant from the Office of Naval Research.

[1] J. Y. Tsao, *Material Fundamentals of Molecular Beam Epitaxy* (World Scientific, Singapore, 1993).
[2] Y. W. Mo, J. Kleiner, M. B. Webb, M. G. Lagally, Phys. Rev. Lett. **66**, 1998 (1991).
[3] J. A. Stroscio, D. T. Pierce, and R. A. Dragoset, Phys. Rev. Lett. **70**, 3615 (1993); J. A. Stroscio and D. T. Pierce, Phys. Rev. B **49**, 8522 (1994).
[4] H. J. Ernst, F. Fabre, and J. Lapujoulade, Phys. Rev. B **46**, 1929 (1992).
[5] R. Q. Hwang, J. Schroder, C. Gunther, and R. J. Behm, Phys. Rev. Lett. **67**, 3279 (1991); R. Q. Hwang and R. J. Behm, J. Vac. Sci. Technol. B **10**, 256 (1992).
[6] W. Li, G. Vidali, and O. Biham, Phys. Rev. B **48**, 8336 (1993).
[7] E. Kopatzki, S. Gunther, W. Nichtl-Pecher, and R. J. Behm, Surf. Sci. **284**, 154 (1993).
[8] G. Rosenfeld, R. Servaty, C. Teichert, B. Poelsema, and G. Comsa, Phys. Rev. Lett. **71**, 895 (1993).
[9] J.-K. Zuo and J. F. Wendelken, Phys. Rev. Lett. **66**, 2227 (1991); J.-K. Zuo, J. F. Wendelken, H. Durr, and C.-L. Liu, *ibid.* **72**, 3064 (1994).
[10] D. D. Chambliss and R. J. Wilson, J. Vac. Sci. Technol. B **9**, 928 (1991); D. D. Chambliss and K. E. Johnson, Phys. Rev. B **50**, 5012 (1994).
[11] Q. Jiang and G. C. Wang, Surf. Sci. **324**, 357 (1995).
[12] F. Tsui, J. Wellman, C. Uher, and R. Clarke, Phys. Rev. Lett. **76**, 3164 (1996).
[13] T. R. Linderoth, S. Horch, E. Laegsgaard, I. Stensgaard, and F. Besenbacher, Phys. Rev. Lett. **78**, 4978 (1997).
[14] J. A. Venables, G. D. Spiller, and M. Hanbucken, Rep. Prog. Phys. **47**, 399 (1984); J. A. Venables, Philos. Mag. **27**, 697 (1973); Phys. Rev. B **36**, 4153 (1987).
[15] F. Family and P. Meakin, Phys. Rev. Lett. **61**, 428 (1988).
[16] J. G. Amar and F. Family, Phys. Rev. Lett. **74**, 2066 (1995).
[17] J. G. Amar, F. Family, and P. M. Lam, Phys. Rev. B **50**, 8781 (1994).
[18] J. G. Amar and F. Family, Thin Solid Films **272**, 208 (1996).
[19] J. G. Amar and F. Family, Surf. Sci. **382**, 170 (1997).
[20] G. S. Bales and D. C. Chrzan, Phys. Rev. B **50**, 6057 (1994).
[21] G. S. Bales and A. Zangwill, Phys. Rev. B **55**, 1973 (1997).
[22] J. A. Blackman and A. Wilding, Europhys. Lett. **16**, 115 (1991).
[23] P. A. Mulheran and J. A. Blackman, Philos. Mag. Lett. **72**, 55 (1995).
[24] J. A. Blackman and P. A. Mulheran, Phys. Rev. B **54**, 11 681 (1996); P. A. Mulheran and J. A. Blackman, Surf. Sci. **376**, 403 (1997).

[25] P. A. Mulheran and D. A. Robbie, Europhys. Lett. **49**, 617 (2000).
[26] C. Ratsch, A. Zangwill, P. Smilauer, and D. D. Vvedensky, Phys. Rev. Lett. **72**, 3194 (1994).
[27] M. C. Bartelt and J. W. Evans, Phys. Rev. B **46**, 12 675 (1992).
[28] M. C. Bartelt and J. W. Evans, J. Vac. Sci. Technol. A **12**, 1800 (1994).
[29] M. C. Bartelt and J. W. Evans, Surf. Sci. **344**, 1193 (1995).
[30] M. C. Bartelt and J. W. Evans, Phys. Rev. B **54**, R17 359 (1996).
[31] M. C. Bartelt, A. K. Schmid, J. W. Evans, and R. Q. Hwang, Phys. Rev. Lett. **81**, 1901 (1998).
[32] J. G. Amar, M. N. Popescu, and F. Family, Surf. Sci. **491**, 239 (2001).
[33] M. N. Popescu, J. G. Amar, and F. Family, Phys. Rev. B **58**, 1613 (1998).
[34] J. G. Amar, M. N. Popescu, and F. Family, Phys. Rev. Lett. **86**, 3092 (2001).
[35] M. von Smoluchowski, Z. Phys. Chem., Stoechiom. Verwandtschaftsl. **17**, 557 (1916); **92**, 129 (1917).
[36] G. Zinsmeister, Thin Solid Films **2**, 497 (1968); **4**, 363 (1969); **7**, 51 (1971).
[37] V. Halpern, J. Appl. Phys. **40**, 4627 (1969).
[38] E. M. Hendricks and M. H. Ernst, J. Colloid Interface Sci. **97**, 176 (1984).
[39] N. V. Brilliantov and P. L. Krapivsky, J. Phys. A **24**, 4787 (1991).
[40] The exact term to account for the monomer-monomer collision rate in Eqs. (6)–(8) is $(Rn_1^2/N_1)/\xi_1^2$ that leads to a nonlinear diffusion equation which may be solved numerically (see Ref. 41). In order to obtain a linear equation the mean-field approximation Rn_1/ξ_1^2 is used (see also Ref. 20).
[41] A. K. Myers-Beaghton and D. D. Vvedensky, Phys. Rev. B **42**, 5544 (1990).
[42] M. N. Popescu, J. G. Amar, and F. Family (unpublished).
[43] The A dependence of B_A can be neglected because it is much smaller than that due to the terms depending on x_A.
[44] P. A. Mulheran and J. A. Blackman, Phys. Rev. B **53**, 10 261 (1996); M. C. Bartelt, C. R. Stoldt, C. J. Jenks, P. A. Thiel, and J. W. Evans, *ibid.* **59**, 3125 (1999).
[45] Coalescence effects (see Fig. 2) are also important starting at coverages around 0.18. While the KMC simulations naturally include coalescence, the rate equations do not include terms to account for such effects.
[46] The condition $a_0+a_1=1$ is required by the definition of the average capture number along with the normalization of the island-size distribution function.
[47] A decreasing value of $f(0)$ with increasing coverage for irreversible growth of extended islands has been seen previously experimentally (Ref. 3) as well as in KMC simulations. (Ref. 16).
[48] Summing Eq. (36) over all $s \geqslant 2$, without any correction to ensure that the normalization condition $\int_0^\infty dA\, G_s(\theta;A)=N_s$ is satisfied, one obtains $G(A)=(1/A^2)H(A-1/N)$, where $H(z)$ is the Heaviside step function. While this distribution satisfies the normalization condition $\int_0^\infty dA\, G(A)=N$, it has very little resemblance to the correct Voronoi-area distribution and leads to a divergent average Voronoi area.
[49] D. D. Vvedensky, Phys. Rev. B **62**, 15 435 (2000).